Biomedical Optics EXPRESS

Focal switching of photochromic fluorescent proteins enables multiphoton microscopy with superior image contrast

Ya-Ting Kao, Xinxin Zhu, Fang Xu, and Wei Min*

Department of Chemistry, Columbia University, New York, NY 10027, USA
**wm2256@columbia.edu*

Abstract: Probing biological structures and functions deep inside live organisms with light is highly desirable. Among the current optical imaging modalities, multiphoton fluorescence microscopy exhibits the best contrast for imaging scattering samples by employing a spatially confined nonlinear excitation. However, as the incident laser power drops exponentially with imaging depth into the sample due to the scattering loss, the out-of-focus background eventually overwhelms the in-focus signal, which defines a fundamental imaging-depth limit. Herein we significantly improve the image contrast for deep scattering samples by harnessing reversibly switchable fluorescent proteins (RSFPs) which can be cycled between bright and dark states upon light illumination. Two distinct techniques, multiphoton deactivation and imaging (MPDI) and multiphoton activation and imaging (MPAI), are demonstrated on tissue phantoms labeled with Dronpa protein. Such a focal switch approach can generate pseudo background-free images. Conceptually different from wave-based approaches that try to reduce light scattering in turbid samples, our work represents a molecule-based strategy that focused on imaging probes.

OCIS codes: (180.4315) Nonlinear microscopy; (180.2520) Fluorescence microscopy; (190.4180) Multiphoton processes.

References and links

1. W. Denk, J. H. Strickler, and W. W. Webb, "Two-photon laser scanning fluorescence microscopy," Science **248**(4951), 73–76 (1990).
2. W. R. Zipfel, R. M. Williams, and W. W. Webb, "Nonlinear magic: multiphoton microscopy in the biosciences," Nat. Biotechnol. **21**(11), 1369–1377 (2003).
3. F. Helmchen and W. Denk, "Deep tissue two-photon microscopy," Nat. Methods **2**(12), 932–940 (2005).
4. J. N. D. Kerr and W. Denk, "Imaging in vivo: watching the brain in action," Nat. Rev. Neurosci. **9**(3), 195–205 (2008).
5. B. R. Masters and P. T. C. So, eds., *Handbook of Biomedical Nonlinear Optical Microscopy* (Oxford University Press, 2008).
6. R. Yuste, ed., *Imaging: A Laboratory Manual* (Cold Spring Harbor Press, 2010).
7. J. Ying, F. Liu, and R. R. Alfano, "Spatial distribution of two-photon-excited fluorescence in scattering media," Appl. Opt. **38**(1), 224–229 (1999).
8. P. Theer, M. T. Hasan, and W. Denk, "Two-photon imaging to a depth of 1000 μm in living brains by use of a Ti:Al_2O_3 regenerative amplifier," Opt. Lett. **28**(12), 1022–1024 (2003).
9. P. Theer and W. Denk, "On the fundamental imaging-depth limit in two-photon microscopy," J. Opt. Soc. Am. A **23**(12), 3139–3149 (2006).
10. D. Kobat, N. G. Horton, and C. Xu, "In vivo two-photon microscopy to 1.6-mm depth in mouse cortex," J. Biomed. Opt. **16**(10), 106014 (2011).
11. N. J. Durr, C. T. Weisspfennig, B. A. Holfeld, and A. Ben-Yakar, "Maximum imaging depth of two-photon autofluorescence microscopy in epithelial tissues," J. Biomed. Opt. **16**(2), 026008 (2011).
12. M. Rueckel, J. A. Mack-Bucher, and W. Denk, "Adaptive wavefront correction in two-photon microscopy using coherence-gated wavefront sensing," Proc. Natl. Acad. Sci. U.S.A. **103**(46), 17137–17142 (2006).
13. N. Ji, D. E. Milkie, and E. Betzig, "Adaptive optics via pupil segmentation for high-resolution imaging in biological tissues," Nat. Methods **7**(2), 141–147 (2010).

#169563 - $15.00 USD Received 30 May 2012; revised 17 Jun 2012; accepted 19 Jun 2012; published 27 Jul 2012

14. D. Kobat, M. E. Durst, N. Nishimura, A. W. Wong, C. B. Schaffer, and C. Xu, "Deep tissue multiphoton microscopy using longer wavelength excitation," Opt. Express **17**(16), 13354–13364 (2009).
15. Z. Yaqoob, D. Psaltis, M. S. Feld, and C. Yang, "Optical phase conjugation for turbidity suppression in biological samples," Nat. Photonics **2**(2), 110–115 (2008).
16. H. Hama, H. Kurokawa, H. Kawano, R. Ando, T. Shimogori, H. Noda, K. Fukami, A. Sakaue-Sawano, and A. Miyawaki, "Sca*l*e: a chemical approach for fluorescence imaging and reconstruction of transparent mouse brain," Nat. Neurosci. **14**(11), 1481–1488 (2011).
17. A. Leray, K. Lillis, and J. Mertz, "Enhanced background rejection in thick tissue with differential-aberration two-photon microscopy," Biophys. J. **94**(4), 1449–1458 (2008).
18. N. Chen, C.-H. Wong, and C. J. Sheppard, "Focal modulation microscopy," Opt. Express **16**(23), 18764–18769 (2008).
19. J. Lippincott-Schwartz and G. H. Patterson, "Photoactivatable fluorescent proteins for diffraction-limited and super-resolution imaging," Trends Cell Biol. **19**(11), 555–565 (2009).
20. D. M. Chudakov, M. V. Matz, S. Lukyanov, and K. A. Lukyanov, "Fluorescent proteins and their applications in imaging living cells and tissues," Physiol. Rev. **90**(3), 1103–1163 (2010).
21. B. Wu, K. D. Piatkevich, T. Lionnet, R. H. Singer, and V. V. Verkhusha, "Modern fluorescent proteins and imaging technologies to study gene expression, nuclear localization, and dynamics," Curr. Opin. Cell Biol. **23**(3), 310–317 (2011).
22. R. Ando, H. Mizuno, and A. Miyawaki, "Regulated fast nucleocytoplasmic shuttling observed by reversible protein highlighting," Science **306**(5700), 1370–1373 (2004).
23. M. Hofmann, C. Eggeling, S. Jakobs, and S. W. Hell, "Breaking the diffraction barrier in fluorescence microscopy at low light intensities by using reversibly photoswitchable proteins," Proc. Natl. Acad. Sci. U.S.A. **102**(49), 17565–17569 (2005).
24. C. Flors, J. Hotta, H. Uji-i, P. Dedecker, R. Ando, H. Mizuno, A. Miyawaki, and J. Hofkens, "A stroboscopic approach for fast photoactivation-localization microscopy with Dronpa mutants," J. Am. Chem. Soc. **129**(45), 13970–13977 (2007).
25. M. Andresen, A. C. Stiel, J. Fölling, D. Wenzel, A. Schönle, A. Egner, C. Eggeling, S. W. Hell, and S. Jakobs, "Photoswitchable fluorescent proteins enable monochromatic multilabel imaging and dual color fluorescence nanoscopy," Nat. Biotechnol. **26**(9), 1035–1040 (2008).
26. E. H. Rego, L. Shao, J. J. Macklin, L. Winoto, G. A. Johansson, N. Kamps-Hughes, M. W. Davidson, and M. G. L. Gustafsson, "Nonlinear structured-illumination microscopy with a photoswitchable protein reveals cellular structures at 50-nm resolution," Proc. Natl. Acad. Sci. U.S.A. **109**(3), E135–E143 (2012).
27. M. Heilemann, P. Dedecker, J. Hofkens, and M. Sauer, "Photoswitches: key molecules for subdiffraction-resolution fluorescence imaging and molecular quantification," Laser Photon. Rev. **3**(1-2), 180–202 (2009).
28. K. Isobe, A. Suda, H. Hashimoto, F. Kannari, H. Kawano, H. Mizuno, A. Miyawaki, and K. Midorikawa, "High-resolution fluorescence microscopy based on a cyclic sequential multiphoton process," Biomed. Opt. Express **1**(3), 791–797 (2010).
29. G. Marriott, S. Mao, T. Sakata, J. Ran, D. K. Jackson, C. Petchprayoon, T. J. Gomez, E. Warp, O. Tulyathan, H. L. Aaron, E. Y. Isacoff, and Y. Yan, "Optical lock-in detection imaging microscopy for contrast-enhanced imaging in living cells," Proc. Natl. Acad. Sci. U.S.A. **105**(46), 17789–17794 (2008).
30. S. Mao, R. K. P. Benninger, Y. Yan, C. Petchprayoon, D. Jackson, C. J. Easley, D. W. Piston, and G. Marriott, "Optical lock-in detection of FRET using synthetic and genetically encoded optical switches," Biophys. J. **94**(11), 4515–4524 (2008).
31. F. V. Subach, L. Zhang, T. W. J. Gadella, N. G. Gurskaya, K. A. Lukyanov, and V. V. Verkhusha, "Red fluorescent protein with reversibly photoswitchable absorbance for photochromic FRET," Chem. Biol. **17**(7), 745–755 (2010).
32. Y.-T. Kao, X. Zhu, and W. Min, "Protein-flexibility mediated coupling between photoswitching kinetics and surrounding viscosity of a photochromic fluorescent protein," Proc. Natl. Acad. Sci. U.S.A. **109**(9), 3220–3225 (2012).
33. R. Ando, C. Flors, H. Mizuno, J. Hofkens, and A. Miyawaki, "Highlighted generation of fluorescence signals using simultaneous two-color irradiation on Dronpa mutants," Biophys. J. **92**(12), L97–L99 (2007).
34. M. Andresen, A. C. Stiel, S. Trowitzsch, G. Weber, C. Eggeling, M. C. Wahl, S. W. Hell, and S. Jakobs, "Structural basis for reversible photoswitching in Dronpa," Proc. Natl. Acad. Sci. U.S.A. **104**(32), 13005–13009 (2007).
35. M. Drobizhev, N. S. Makarov, S. E. Tillo, T. E. Hughes, and A. Rebane, "Two-photon absorption properties of fluorescent proteins," Nat. Methods **8**(5), 393–399 (2011).
36. T. Grotjohann, I. Testa, M. Leutenegger, H. Bock, N. T. Urban, F. Lavoie-Cardinal, K. I. Willig, C. Eggeling, S. Jakobs, and S. W. Hell, "Diffraction-unlimited all-optical imaging and writing with a photochromic GFP," Nature **478**(7368), 204–208 (2011).
37. L. Wei, Z. Chen, and W. Min, "Stimulated emission reduced fluorescence microscopy: a concept for extending the fundamental depth limit of two-photon fluorescence imaging," Biomed. Opt. Express **3**(6), 1465–1475 (2012).

#169563 - $15.00 USD Received 30 May 2012; revised 17 Jun 2012; accepted 19 Jun 2012; published 27 Jul 2012

1. Introduction

Multiphoton fluorescence microscopy is now the most popular technique for imaging scattering biological samples with sub-cellular resolution [1,2]. Due to the nonlinear intensity dependence of the absorption process, multiphoton excited fluorescence is mostly generated from the laser focus where the probability of having two (or more) simultaneous incident photons is the highest. This confined excitation enables efficient capture of scattered fluorescence photons by a wide-field detector without a confocal pinhole. Such intrinsic optical sectioning dramatically improves the detection sensitivity and hence imaging depth into scattering samples [3,4]. Consequently, multiphoton microscopy has become an indispensable tool for biomedicine [5,6].

However, multiphoton microscopy will eventually lose contrast when imaging deep into scattering samples [7–11]. As demonstrated in Fig. 1(A), the two-photon fluorescence image of fluorescent beads embedded in a turbid 3D sample quickly fades away with the increasing depth. But images can be acquired much deeper if the laser power is increased to compensate for the scattering loss as shown in Fig. 1(B). Nevertheless, image contrast deteriorates with depth as the fluorescence from the out-of-focus beads grows and eventually dominates the signal from the focal region. At this fundamental depth limit, the inherent optical sectioning breaks down. Obviously, this loss of image contrast cannot be overcome by further increasing the excitation efficiency which would enhance signal and background equally.

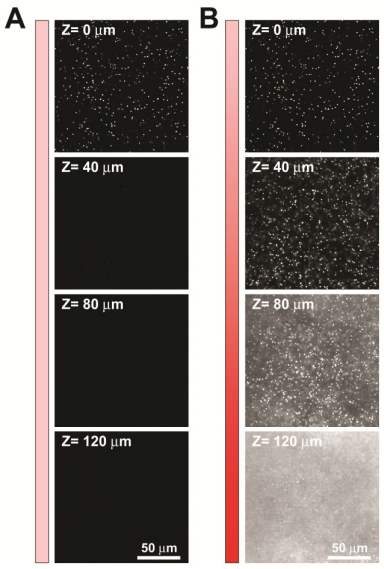

Fig. 1. Fundamental imaging-depth limit of multi-photon fluorescence microscopy. (*A*) Depth-dependent two-photon optical sections of a tissue phantom made of 5% intralipid, 2% agarose gel and fluorescent beads (diameter 0.9 μm) under a constant laser power excitation. Fluorescence signal quickly attenuates with the imaging depth. (*B*) Depth images of the same sample using a compensative higher laser power to maintain the signal strength. The resulting images can reach deeper than (*A*), but their contrast deteriorates as the out-of-focus background begins to dominate. The fundamental imaging-depth limit is defined when the in-focus signal and the out-of-focus background are equal to each other.

Extensive efforts have been invested in improving the image contrast of multiphoton microscopy by employing a number of strategies, such as adaptive optics to pre-compensate for the scattering loss [12,13], imaging with longer wavelengths [14], optical phase conjugation [15], *ex vivo* chemical cleaning reagent [16], differential aberration imaging [17] and focal modulation [18]. It is worth noting that many of these methods focus on tailoring the incident laser beams to reduce the scattering effect (including the tissue induced aberration

#169563 - $15.00 USD Received 30 May 2012; revised 17 Jun 2012; accepted 19 Jun 2012; published 27 Jul 2012

and refractive index mismatch) of the turbid sample on the light waves. Relative little work has been carried out to search for special imaging probes themselves.

Herein we explore the utility of an emerging class of reversibly switchable fluorescent proteins (RSFPs) for high-contrast multiphoton imaging. GFP and its variants are widely used as genetically encoded reporters in bio-imaging [19–21]. Unlike conventional FPs, RSFPs can switch between a fluorescent and a non-fluorescent state upon light illumination in a reversible manner. Such unique photochromism has been employed for a variety of applications including studying intracellular protein trafficking [22], sub-diffraction resolution fluorescence microscopy [23–28], removing auto-fluorescence via optical lock-in [29], photochromic FRET [30,31], and most recently as a genetically encoded micro-viscosity reporter [32]. By harnessing the switching ability of RSFPs, our strategy preferentially turns on or off the RSFPs at the focal plane while keeping the protein in the out-of-focus background in the opposite state. We demonstrate two distinct techniques, multiphoton deactivation and imaging (MPDI) and multiphoton activation and imaging (MPAI), on tissue phantoms made of live bacterial and mammalian cells labeled with Dronpa-3.

2. Results and discussions

Dronpa and its closely-related mutants Dronpa-2 and Dronpa-3 are among the first discovered and best studied RSFPs. In this report we chose to use Dronpa-3 for demonstration, as it exhibits a higher quantum yield of bright-to-dark switching when compared to the original Dronpa [33]. Like most RSFPs, Dronpa-3 is initially in its bright state. As shown in Fig. 2(A), irradiating Dronpa-3 at 488nm will generate green fluorescence emission. However, prolonged 488nm illumination converts Dronpa-3 to a dark state. Then irradiation at 405nm efficiently recovers the original bright-state. The structural basis for its photochromism is believed to be the *cis-trans* isomerization of the internal chromophore, accompanied by a change in the protonation state [34].

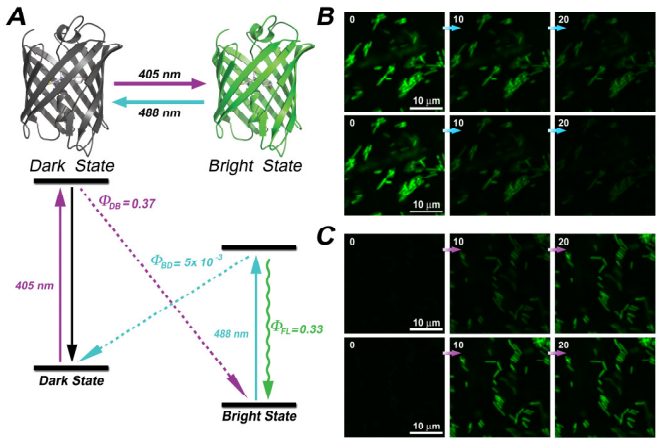

Fig. 2. One-photon and two-photon induced photoswitching of Dronpa-3 protein. (A) Upon irradiation at 405 and 488 nm, Dronpa-3 switches between dark and bright states in a reversible manner (cyan and purple dashed lines), where the downward black arrow and green arrow indicates the non-radiative relaxation from the excited dark state and florescence decay from the excited bright state, respectively. (B) Time-lapse (in seconds) two-photon images (at 920nm) of Dronpa-3 expressing *E. coli* cells undergoing bright-to-dark switching upon the same 920nm irradiation. A two-times higher 920nm laser power leads to notably faster switching-off kinetics (*lower panel*). (C) Time-lapse (in seconds) two-photon images (at 920nm) of Dronpa-3 expressing *E. coli* cells undergoing dark-to-bright switching upon 800nm irradiation (applied between adjacent images). A two-times higher 800nm laser power leads to notably faster switching-on kinetics (*lower panel*).

#169563 - $15.00 USD Received 30 May 2012; revised 17 Jun 2012; accepted 19 Jun 2012; published 27 Jul 2012

We then evaluate two-photon induced photoswitching kinetics of Dronpa-3. Figure 2(B) shows the two-photon fluorescence images of Dronpa-3 expressing *E. coli* cells excited by a pulsed laser at 920nm which is around the two-photon absorption peak of GFP [35]. Repeated scanning and imaging over the same cells displays a graduate signal attenuation due to the bright-to-dark switching. As expected, a higher 920nm laser power leads to a notably faster kinetics of switching-off. In both tests, brief irradiation at 405nm subsequently recovers the original bright-state intensity. Hence, the bright-to-dark switching-off kinetics is indeed dependent on the two-photon excitation intensity at 920nm. Similarly, in Fig. 2(C), we confirmed that the dark-to-bright switching-on kinetics is dependent on the two-photon excitation intensity at 800nm. Therefore, RSFPs offer on-off molecular states that can be modulated by external two-photon light illumination.

Before elaborating on MPDI and MPAI, we need to first discuss two-photon imaging of regular fluorophores. Using the criterion that the in-focus signal (S) and the out-of-focus background (B) are equal [7–11], the fundamental depth limit can be defined as

$$\left(\frac{S}{B}\right)_{regular} = \frac{\int_{V_{in}}\int_0^{\tau} C_S(r,z)I^2(r,z,t)\,\mathrm{d}t\,\mathrm{d}V}{\int_{V_{out}}\int_0^{\tau} C_B(r,z)I^2(r,z,t)\,\mathrm{d}t\,\mathrm{d}V} = 1 \qquad (1)$$

where V_{in}, is the focal volume, V_{out}, is the total sample volume along the beam path but excluding the focal volume, r, is the distance from the optical axis, z, is the axial distance from the surface, C is the local fluorophore concentration, and I is the laser intensity, and τ is the pixel dwell time. We assume there is no fluorophore saturation or bleaching, and identical fluorescence collection efficiency between the signal and the background at the wide-field detector.

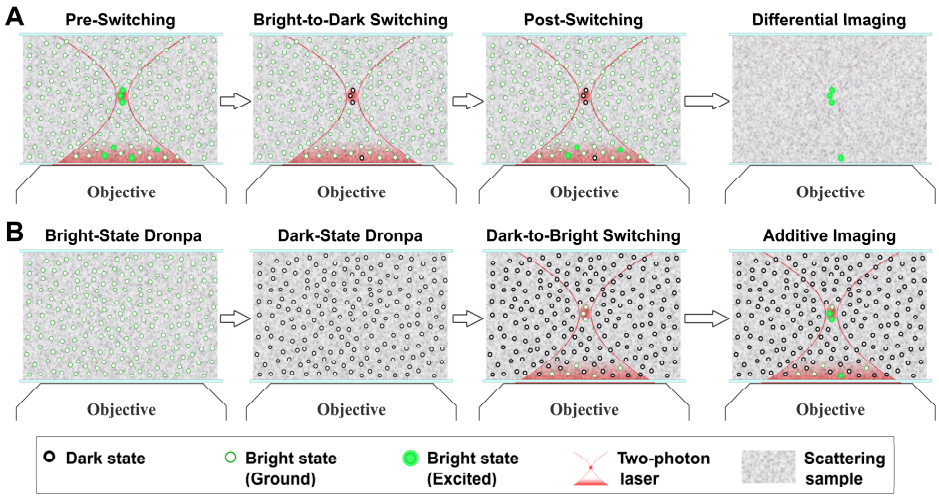

Fig. 3. Principles of multiphoton deactivation and imaging (MPDI) and multiphoton activation and imaging (MPAI) with RSFPs. (A) MPDI. For the regular pre-switching image, when imaging deep into the scattering sample, substantial laser intensity is distributed out of focus, generating background that is comparable to the in-focus signal. In the post-switching image, in-focus RSFPs are switched off much more than those out of focus, creating a disparity of dark-bright states in space. The resulting difference image leads to significantly improved contrast. (B) MPAI. RSFPs which are originally in the bright state will be completely switched off into the dark state. The subsequent multiphoton activation will switch on a higher percentage of RSFPs at focus than those out of focus. This spatial disparity of dark-bright transitions leads to a significantly decreased background in the final multiphoton imaging step.

#169563 - $15.00 USD Received 30 May 2012; revised 17 Jun 2012; accepted 19 Jun 2012; published 27 Jul 2012

Equation (1) could help us to quantify how the laser intensity distributes within the scattering sample when the above fundamental depth limit is reached. The fluorophores are normally distributed throughout the 3D volume of the sample. Thus, the number of out-of-focus fluorophores is almost always orders-of-magnitude larger than that of the in-focus ones. Therefore, if the generated fluorescence signal is comparable between the focal volume and the out-of-focus volume, the laser intensity at the focus will have to be much more intense than the out-of-focus counterpart, despite the scattering loss. When coupled with photoswitching transitions, the high focal laser intensity could offer additional discrimination mechanisms against background, which is exactly being employed in MPDI and MPAI.

We now propose to carry out MPDI as shown in Fig. 3(A): make a differential image before and after switching off the bright Dronpa-3 preferentially at the focus volume. The *pre*-deactivation image of Dronpa-3 labeled sample, quickly acquired at 920 nm, would be the same as the image obtained with regular GFP. In contrast, the *post*-deactivation image will depend on the switching kinetics whose rate should be dependent on the local intensity of 920nm (Fig. 2(B)). As analyzed earlier for Eq. (1), the 920nm laser intensity at the focus is much more intense than the out-of-focus counterpart at the imaging-depth limit. In a non-depletion region, this would lead to a more efficient deactivation at the focus after the switching scanning process at 920nm. Consequently, as illustrated by Fig. 3(A), Dronpa-3 will be primarily turned off at the focus in the post-deactivation image. The resulting difference image between *pre-* and *post-* deactivation would effectively cancel the out-of-focus background. Therefore, we expect a much improved *S*/*B* ratio for MPDI with Dronpa-3.

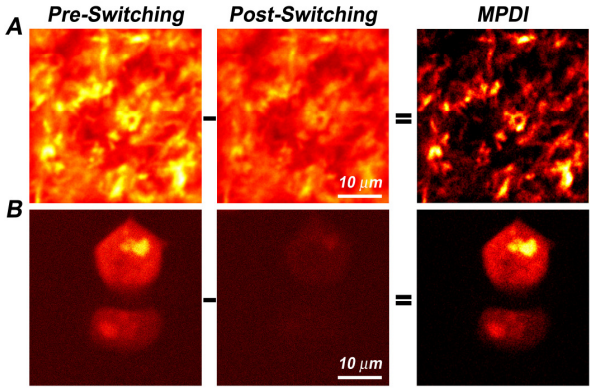

Fig. 4. Experimental demonstration of multiphoton deactivation and imaging (MPDI) on tissue phantoms. (A) For Dronpa-3 expressing *E. coli* cells packed in 3D, the regular pre-switching image (at 920nm) is overwhelming at a depth of 250 μm. After performing a slow deactivation scanning, the post-deactivation image is dimmer. The difference image (after auto-scaled) offers a much improved image contrast. (B) Similar contrast improvement is observed for HEK 293T cells (transfected by H2B-Dronpa-3 plasmids) placed on a dense layer of scattering *E. coli* cells expressing Dronpa-3.

We then demonstrate MPDI on tissue phantoms made of live bacterial or mammalian cells. Dronpa-3 expressing *E. coli* cells are embedded in 3D low melting-point agarose gel (2%). The resulting sample is highly scattering due to the packed *E. coli* cells in 3D. As demonstrated in Fig. 4(A), the out-of-focus background is substantial for a quick pre-switching scan at a depth of 250 μm. The corresponding near-unity *S*/*B* indicates that this depth is close to the fundamental imaging-depth limit for regular fluorophores. After performing one relatively slow (or multiple fast) deactivation scanning at 920nm, the post-deactivation image indeed became dimmer. The difference image offers a satisfactory contrast with much reduced out-of-focus background. We note that prolonged deactivation led to poor MPDI contrast due to depletion within the whole sample. To demonstrate MPDI in mammalian cells, we further constructed a "two-layer" composite sample in which a dense

#169563 - $15.00 USD Received 30 May 2012; revised 17 Jun 2012; accepted 19 Jun 2012; published 27 Jul 2012

layer (120 μm) of Dronpa-3 expressing *E. coli* cells serve as the "scattering" background and H2B-Dronpa-3 expressed HEK 293T cells on a coverslip are the targeted objects. As shown in Fig. 4(B), the MPDI image is effectively free from out-of-focus background generated from the *E. coli* cells in the "scattering" layer.

Inspired by the spirit of MPDI, we now propose a different but related technique: multiphoton activation and imaging (MPAI) with RSFPs. This is possible because of the reversible manner of the *cis-trans* isomerization. As shown in Fig. 3(B), we will implement three sequential steps: first, switching Dronpa-3 in the entire sample volume of interest to the dark state with a prolonged 488 nm illumination; second, preferentially activating Dronpa-3 from the focus to the bright states by scanning the focal plane with a pulsed laser at 800 nm with a proper pixel dwell time of ξ; third, taking a regular two-photon image at 920 nm. Similar to the deactivation in MPDI, the two-photon activation process will occur predominately at the focal plane in a non-saturation region, and therefore, the subsequent two-photon imaging of the photoactivated population should exhibit a superior image contrast.

MPAI is demonstrated on similar tissue phantom samples as in MPDI. As shown in Fig. 5(A), the out-of-focus background is overwhelming for the regular two-photon images of the Dronpa-3 (bright state) expressing *E. coli* cells at a depth of 140μm. A brief 488nm laser illumination efficiently switched off Dronpa-3 completely in the sample volume. After that, two-photon activation by scanning with a 800nm pulsed laser and subsequent two-photon imaging with a 920nm pulsed laser resulted in a remarkable image contrast of cells at the focal plane. We note that over-activation (with too strong 800nm laser or too slow scanning) led to poor MPAI contrast. The result on H2B-Dronpa transfected HEK 293T cells in the "two-layer" sample, shown in Fig. 5(B), also proves a much lower background and improved contrast for chromosome features inside the cell nucleus. Thus, we have demonstrated MAPI in providing superior contrast and hence deeper penetration of two-photon microscopy for scattering samples.

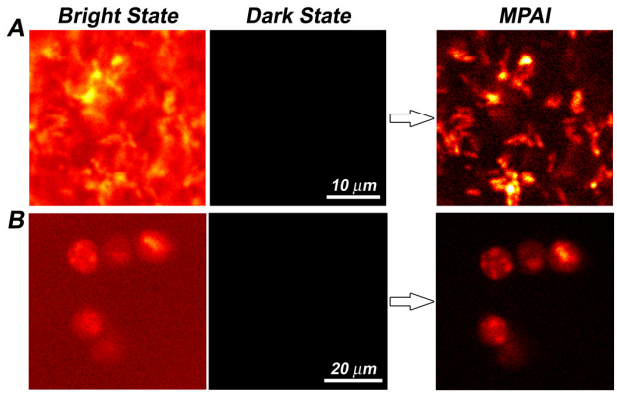

Fig. 5. Experimental demonstration of multiphoton activation and imaging (MPAI) on tissue phantoms. (A) For Dronpa-3 expressing *E. coli* cells mixed with polystyrene beads packed in 3D, the background in the bright-state image (at 920nm) is overwhelming at a depth of 140μm. A brief 488nm laser illumination converted Dronpa-3 in the volume of interest completely to the dark state. Afterwards, a relatively weak 800nm pulsed laser was used to activate Dronpa-3 prior to the subsequent two-photon imaging at 920nm. The resulting MPAI image reveals features that are buried in the original image of the bright state. (B) Similar contrast improvement is observed for HEK 293T cells (transfected by H2B-Dronpa plasmids) placed on a 120μm-thick layer of Dronpa-3 expressing *E. coli* cells.

3. Experimental details

In Fig. 1, fluorescent beads were purchased from Invitrogen (F13080: blue/green 1.0 μm beads), mixed with 5% Intralipid (Sigma I141) which serves as the scattering species, and then embedded in 2% agarose gel in three dimension. In live bacteria imaging experiments

#169563 - $15.00 USD Received 30 May 2012; revised 17 Jun 2012; accepted 19 Jun 2012; published 27 Jul 2012

presented in Figs. 2, 4, and 5, Dronpa-3 expressing *E. coli* cells were prepared as previous reported [32], and then harvested by centrifugation, resuspended and embedded inside an imaging spacer using 2% agarose gel with or without non-fluorescent polystyrene beads (0.9 μm diameter in average from Sigma-Aldrich *CLB9*). In the HEK 293T mammalian cell imaging experiments presented in Figs. 4 and 5, "two-layer" composite samples consisting of a background layer and a target layer were prepared as follows. An imaging spacer with a 120 μm thickness (Sigma *GBL654004*) was first pasted onto a piece of micro coverglass (VWR 48393-150). Inside the spacer, 10 μL of Dronpa-3 expressing *E. coli* cells in 2% agarose gel together with non-fluorescent beads serving as the scattering background was added. This background material was then sealed inside the spacer by a 35-mm glass bottom petri dish on the top. The imaging target objects, HEK 293T cells, were cultured on the petri dish and transiently transected with H2B-Dronpa-3 plasmids which were constructed as reported previously [32].

All the two-photon fluorescence images were taken on a Leica TCS SP5 MP inverted microscope equipped with a Mai Tai HP laser (690-1040 nm tunable emission) and a HCX PL APO CS 20X DRY microscope objective (N.A. = 0.70). A non-descanned epi photomultiplier tube (PMT) detector placed directly behind the objective was used for fluorescence collection in combination with a 680 nm Short Pass emission filter. Images were processed with LAS AF software unless otherwise stated.

Images of fluorescent beads (Fig. 1) were taken under 840 nm with a pixel dwell time of 20 μs. Images of the Dronpa-3 expressing *E. coli* samples (Figs. 4(A) and 5(A)) were taken under 920 nm (99 mW) with a pixel dwell time of 40 μs. For Fig. 4(A), a slow deactivation scanning in x-y at 920 nm (99 mW) with a pixel dwell time 160 μs was performed before taking the post-deactivation image. For Fig. 5(A), an activation scanning in x-y at 800 nm (2.9 mW) with a pixel dwell time of 80 μs were performed in prior to the subsequent imaging at 920 nm. The pre-deactivation images of H2B-Dronpa-3 transfected HEK 293T samples (Fig. 4(B)) were taken under 920 nm (99 mW) with a pixel dwell time of 40 μs. The post-deactivation image, after 40 frames of two-photon deactivation scanning at 920nm (99 mW), was taken under 920 nm (99 mW) with a pixel dwell time of 40 μs. Images of H2B-Dronpa transfected HEK293T samples (Fig. 5(B)) were taken under 920 nm with a pixel dwell time of 40 μs. The two-photon activation was performed with 4 scanning frames of 800 nm (40 mW) with a pixel dwell time of 40 μs. Note that due to the strong sample scattering of the prepared tissue phantoms, the actual laser power reached at the actual focal plane is lower than the measured total power transmitted through the microscope objective. All images were acquired with 512 by 512 pixels.

4. Conclusion

Both MPDI and MPAI of RSFPs are based on the insight that the laser intensity at the focus has to be much more intense than the out-of-focus counterpart despite the scattering loss, when the depth limit is reached for regular fluorophores as defined in Eq. (1). When coupled to the photoswitching kinetics of RSFPs, such laser intensity disparity translates to an additional mechanism for discriminating signal over background in the non-depletion or saturation region. Hence, although MPDI and MPAI seem to adopt opposite approaches, the *S/B* are comparable between MPDI and MPAI in theory. However, there is a profound difference in terms of noise. The background rejection is performed numerically in MPDI, after detection, rather than physically, before detection as in MPAI. Although the average position-dependent backgrounds can be effectively canceled out for every scanning pixel in MPDI, the shot noises from the two backgrounds would add in quadrature, which sets a higher limit for the distinguishable in-focus signal size for MPDI.

Radically different from the existing approaches that mostly focus on reducing scattering loss by tailoring the incident light waves, the current work represents a molecule-based strategy that harnesses the special photophysics of imaging probes themselves. In terms of

#169563 - $15.00 USD Received 30 May 2012; revised 17 Jun 2012; accepted 19 Jun 2012; published 27 Jul 2012

practical performance, the recently engineered new generation of RSFPs [31,36] with high photon output, faster photoswitching rate and different colors has the prospect to further improve MPDI and MPAI.

Finally, it is constructive to make connections to a few other related techniques. Cyclic sequential transition of Dronpa-3 has been harnessed to increase the spatial resolution in one-photon imaging [28]. In addition, the switching of RSFPs was used to improve the image contrast in the optical lock-in detection [29]. However, the background there is mainly from the auto-fluorescence which cannot be modulated by light. Moreover, the recently proposed stimulated emission reduced fluorescence (SERF) microscopy can also improve the image contrast for thick scattering samples [37]. From a spectroscopy perspective, MPDI of RSFPs is very similar to the attenuation effect of stimulated emission in SERF microscopy.

Acknowledgments

We thank Lu Wei, Zhixing Chen, Louis Brus, Rafael Yuste, Darcy Peterka and Virginia Cornish for helpful discussions. W.M. acknowledges the startup funds from Columbia University, and grant support from Kavli Institute for Brain Science.